Castable solid pressure media for multianvil devices

David Walker, and Jie Li ⓘD

COLLECTIONS

Paper published as part of the special topic on High Pressure Science
Note: This paper is part of the special issue on High Pressure Science.

View Online   **Export Citation**   **CrossMark**

ARTICLES YOU MAY BE INTERESTED IN

New developments in high-pressure X-ray diffraction beamline for diamond anvil cell at SPring-8
Matter and Radiation at Extremes **5**, 018403 (2020); https://doi.org/10.1063/1.5126038

Chemistry under extreme conditions: Pressure evolution of chemical bonding and structure in dense solids
Matter and Radiation at Extremes **5**, 018202 (2020); https://doi.org/10.1063/1.5127897

 Understanding the effects of radiative preheat and self-emission from shock heating on equation of state measurement at 100s of Mbar using spherically converging shock waves in a NIF hohlraum
Matter and Radiation at Extremes **5**, 018401 (2020); https://doi.org/10.1063/1.5131748

Matter and Radiation at Extremes

SPECIAL ISSUE: Z-pinches

READ NOW!

Castable solid pressure media for multianvil devices

View Online · Export Citation · CrossMark

David Walker[1] and Jie Li[2] (iD)

AFFILIATIONS

[1] Lamont-Doherty Earth Observatory, Columbia University, Palisades New York 10964, USA
[2] Earth and Environmental Sciences, University of Michigan, Ann Arbor Michigan 48109, USA

Note: This paper is part of the special issue on High Pressure Science

ABSTRACT

Castable solids from Aremco (http://www.aremco.com/potting-casting-materials/) are convenient media for pressure transmission in multianvil geometries of complex shape. A zirconia-based castable ceramic, Aremco Ceramacast 646, is introduced and compared to MgO-Al_2O_3-SiO_2-based Aremco Ceramacast 584. Ceramacast 646 has some advantages over the widely used Ceramacast 584; these include ease of consistent fabrication and better thermal insulation. Some disadvantages are poorer efficiency in converting press thrust to sample pressure and slower quenching rates. Potential applications are informed by these differences.

INTRODUCTION

Generating high pressures for phase equilibrium studies, material synthesis, and the investigation of material properties under extreme conditions has led to significant advances in the study of Earth and planetary interiors, solid-state physics and chemistry, and materials sciences. The conversion of motive force to pressure requires a pressure transmitting medium. A simple case is the use of a pump to increase the fluid content within a filled, closed vessel. The fluid is the pressure medium, and the pressures produced are hydrostatic. Gaseous fluids store the mechanical work of compression, so that it becomes increasingly challenging at high compressions to deliver sufficient gas. Gas leaks can release that stored energy unsafely. Liquid pressure media of lower compressibility than gases are thus advantageous at high pressures. However, fluids may encounter freezing at high pressures, in which case the solid pressure media no longer transmit pressure to the vessel contents in a hydrostatic manner. If frozen pressure transmitting media are not too strong in shear, the deviation from hydrostatic pressure may be acceptable. The use of weak deformable solids as pressure transmitting media in very high-pressure devices can be more convenient than fluids. Machinable ceramics like Macor, talc, pyrophyllite, and hexagonal boron nitride have been used as pressure media. Die-formed granular aggregates of NaCl, KCl, $BaCO_3$, and CaF_2 are also used in cylindrical geometry applications.

The multianvil apparatus has been widely used to generate pressures between tens of kilobars (a few gigapascals) up to 1 Mbar, as reviewed by Liebermann.[1] For the more complex shapes of multianvil device pressure media, the use of castable ceramics was introduced by Walker.[2] At that time, a survey of the castable Aremco products led to the adoption of Aremco Ceramacast compound 584 as the ceramic of choice for this application. This choice was largely dictated by the superior performance of Ceramacast 584 regarding its ability to convert press thrust to sample pressurization, as determined by calibration against reference pressure-temperature points, like Bi transitions at room temperature and coesite to stishovite transitions at high temperatures in SiO_2 standard materials. Ceramacast 584 has been used as a multianvil device pressure medium in many laboratories worldwide, including those at the Lamont-Doherty Earth Observatory (LDEO) of Columbia University and University of Michigan. Aremco's changes to the formulation over the years, which has adversely affected performance, has led to their special formulation on request of compound 584, with its original constitution, designated 584-OF, which is used in the multianvil community as a castable ceramic. Experienced users will be only too familiar with some of the characteristics of 584 which are most charitably described as "fussy:" the pot life or setting time is inconveniently short (less than 30 s); the shelf life is annoyingly short (up to six months, thus requiring compensating adjustment of the powder-to-binder ratio as a batch ages); the need to carefully control the humidity of the curing environment and carefully grease the molds to prevent leakage and

facilitate release; the need to cure sufficiently, so that firing at 1050 °C does not lead to cracking and crumbling of finished octahedra; the need for special care against crumbling in machining the octahedra for heater and thermocouple channels; the aggressive wear of tungsten carbide drills; and the poor performance at pressures in excess of 100 kbar (10 GPa) caused by the ductile deformation of weak tungsten carbide anvils and by the brittle failure of strong anvils.

CERAMACAST 646

The difficulties with the Ceramacast 584 pressure medium motivate and inform a search for alternative castable materials for use as pressure media. This report reviews some characteristics of the zirconia-based castable Aremco compound 646. We determine pressurization efficiency, both hot and cold, as well as the thermal structure within LaCrO$_3$ (LCO) heaters that are placed inside 646 octahedra. The pressurization efficiency of 646 is still not competitive with 584, confirming the results from 1991. However, the ~20%–30% lower pressurization efficiencies are compensated by convenience in preparation and fabrication of 646 assemblies compared to the "fussy" 584, including longer pot life (tens of minutes), longer shelf life (years), simpler curing and firing, and excellent structural integrity when machined. Moreover, the zirconia 646 pressure medium is far superior to 584 in its thermal insulation characteristics. Good thermal insulation is desirable for keeping the tungsten carbide anvils cool and for promoting a uniform thermal structure of the payload, but is undesirable for achieving rapid quenching rates. If lower pressurization efficiency and quench rate are acceptable, Aremco Ceramacast 646 provides an attractive alternative to 584 for use as a multianvil device pressure medium.

Although octahedra with precast fins were initially introduced to eliminate the need for making and installing separate pyrophyllite gaskets, the 646 material can be cast as "normal" finless octahedra and be used in combination with pyrophyllite gaskets. Finless 646 offers

an alternative to the finless octahedra from Japan Engineering Co. and the now widely used injection molded octahedra developed by COMPRES,[3] with the advantage of low cost, flexible geometry, and better thermal insulation. Figure 1 shows the various forms in which we have prepared Ceramacast 646 for use as pressure media.

A note on the preparation of Ceramacast 646 for application as a pressure medium in heated experiments: 646 must be rigorously dewatered by heating, just as Ceramacast 584 must be. Ignore the curing recipe on the label supplied by Aremco. Instead, heat the unfired casting at about 1000 °C/hour from room temperature to 1050 °C and hold at 1050 °C for at least an hour. Do not put the casting directly into a 1050 °C furnace as crumbling may occur. Firing for 2 h instead of 1 h does no damage. After a fresh pour of 646 has cured at least overnight in the molds, it can be fired immediately or stored, without any special humidification, for indefinite periods of time before firing. The firing step, whether performed or not, makes no difference to the results of Bi calibrations, but is required for applications at high temperature where water escape during heating can catastrophically destabilize the experiment. Be warned.

CALIBRATIONS

The calibration results are given in the form of sample pressure in kilobar (and gigapascal) vs press load in US tons produced by the application of oil pressure to a hydraulic ram. Other units of pressure may be used in various laboratories. The bar is a metric unit of pressure, defined as exactly equal to 100 000 Pa, which is slightly less than the current average atmospheric pressure on Earth at sea level. The metric ton, also known as "tonne," equals 1000 kg, or approximately 2204 pounds. The US ton, also known as the short ton, is 2000 pounds, whereas the British ton is the long ton, which is 2240 pounds.

IN SITU BI CALIBRATION AT ROOM TEMPERATURE

Table I gives Bi calibration results using the values of Decker *et al.*[4] and Walker[2] for the standard phase transitions in Bi at room temperature. A justification for the "31" kbar choice[2] for Bi II–III is given in the Appendix. The difficulty of not making this choice is illustrated by the open symbols in Fig. 13 of the Appendix.
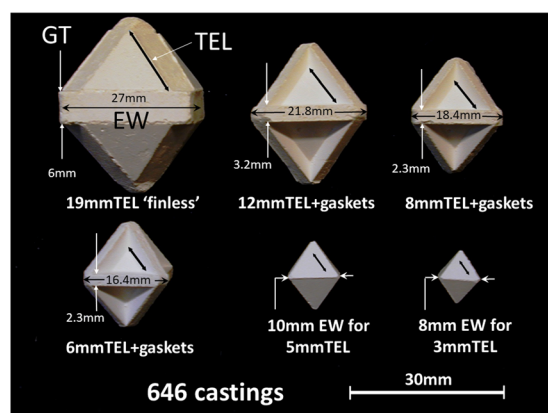

FIG. 1. Ceramacast 646 pressure media for use in multianvil pressurizations. Dimensional abbreviations: TEL = truncated edge length of the triangular corner facet on a tungsten carbide anvil, which will mate to the pressure medium's triangular octahedral face. GT = gasket thickness. EW = equatorial width. Regular octahedra of 10 mm and 8 mm EW without integral cast gaskets are for mating to 5 mm and 3 mm TEL anvils with COMPRES pyrophyllite gaskets.
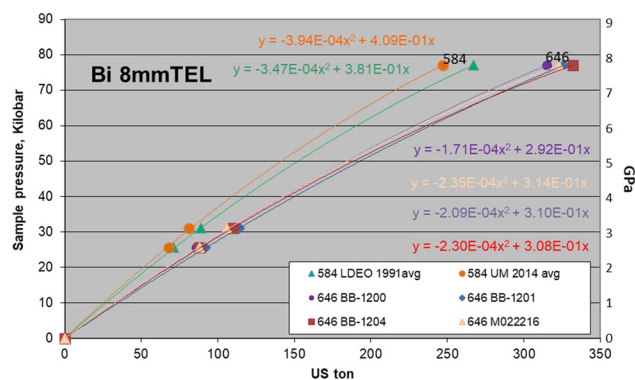

FIG. 2. 8 mm TEL Bi calibrations at room temperature. Ceramacast 646 (red, purple, blue, and pink) are compared with 584 (green and orange).

TABLE I. Room temperature Bi calibration in cast octahedra with integral fin gaskets.
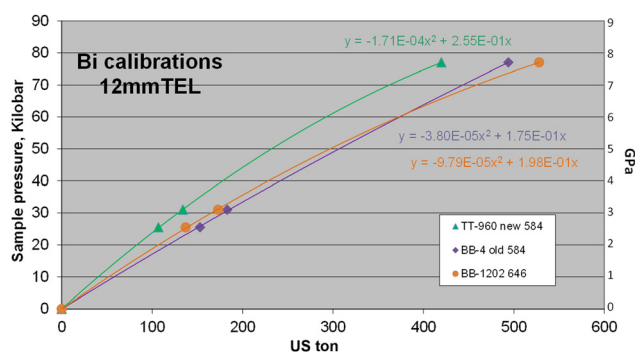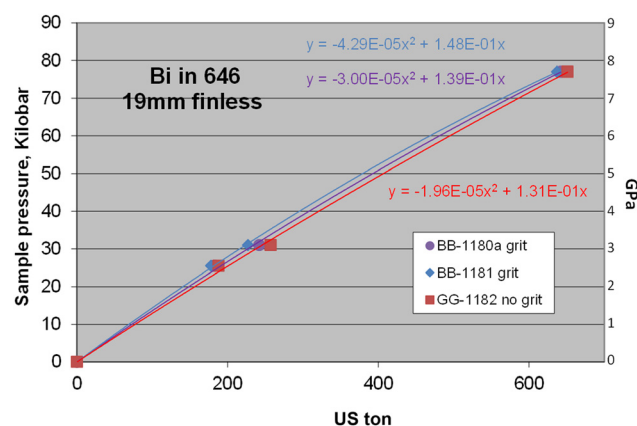
	Pressure → TEL	25.5 I-II[4]	"31" II-III[2]	77 III-V[4]	← Kilobars phase trans
		646 Bi calibrations			
BB-1248	6 mm	55	77	222	US ton
BB-1204	8 mm	88	110	332	US ton
BB-1200	8 mm	86	109	315	US ton
BB-1201	8 mm	92	114	326	US ton
M022216	8 mm	88	106	323	US ton
BB-1202	12 mm	137	173	528	US ton
BB-1180a	19 mm grit	183	242	642	US ton
BB-1181	19 mm grit	178	227	637	US ton
BB-1182	19 mm no grit	188	257	651	US ton
		584 Bi calibrations			
BB-1423	8 mm	86	109	274	US ton
Walker '91	8 mm	71	89	267	US ton
UM 2014	8 mm	68	81	247	US ton
BB-4	12 mm old	153	183	494	US ton
TT-960	12 mm new	107	134	420	US ton

Figure 2 gives some results for room-temperature Bi calibrations for 8 mm truncation-edge-length (TEL). Four 646 experiments cluster tightly at about 320 tons which is about 20% more force needed to reach the old 584 calibrations of Walker[2] shown by the green curve. The sacrifice in pressurization efficiency is compensated by simpler preparation and superior thermal insulation. The small spread of 646 results is typical of the reproducibility of previous the 584 calibration results given by Walker.[2] The reproducibility between LDEO and Michigan is excellent for 646. The reproducibility between the calibrations on 584, done in two different labs 23 years apart, is acceptable, especially considering the fact that casting protocols and materials evolved between 1991 and 2014.

Figure 3 shows the efficiency gap to be a little larger, about 25%, for 12 mm TEL octahedra between 646 (orange curve) and the new 584 (green curve). The old 584 from 1991 (purple curve, like the orange curve) presents concerns regarding long-term quality control in the 584 assemblies. It is unclear whether this is a consequence of within-batch aging, long-term formula or configurational dimension changes, or rogue measurements. We have found some inconsistency with 584's ease of preparation and behavior from batch to batch over the years, which may be another symptom coupled to this variation in efficiency. Recent University of Michigan results for 12 mm TEL 584 efficiency in seven separate experiments achieving the Bi III–V transition at 77 kbar at 426 ± 18 US tons are very comparable to the green curve (77 kbar at 420 tons) for new LDEO 584 in Fig. 3. This suggests that current batches of 584 are reproducible between separate labs, and that the twenty-eight-year-old BB-4 test is different, showing distinctly lower efficiency and curvature in pressurization, probably as a result of the different gasket fin dimensions in our early casting configurations and materials.

For the 19 mm finless assemblies shown in Fig. 4, the reproducibility is excellent and there seems to be no difference whether

FIG. 3. 12 mm TEL Bi calibrations at room temperature. Ceramacast 646 (orange) is compared to 584 (green and purple).

FIG. 4. 19 mm "finless" Bi calibrations at room temperature for Ceramacast 646.
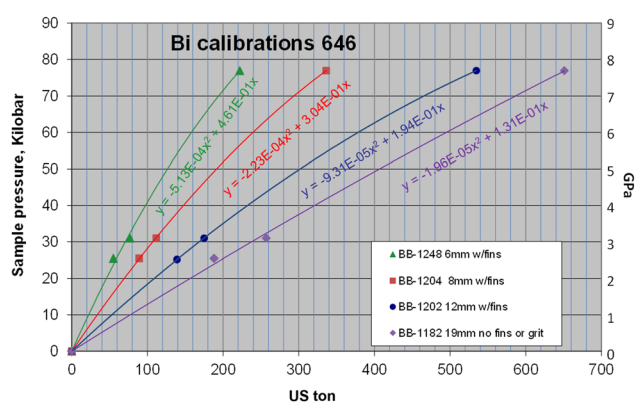
FIG. 5. Summary of Bi calibrations at room temperature in Ceramacast 646.

there is SiC grit in the mix or not. This confirms results from about 20 years ago when we first explored the 19 mm finless 646 configuration, which came with grits that Aremco no longer supplies. There is no 584 for comparison at 19 mm TEL. The finless design in which the pressure medium makes its own gasket by extrusion during compression is very efficient at generating high pressurization in large volumes. We have heated cylinders of ½ in. diameter and ¾ in. length in $LaCrO_3$ heaters to pressures of 70–80 kbar at press loads of less than 800 US tons.

Putting all 646 Bi room temperature results together in Fig. 5 gives a useful guide to 646 performance with the dimensional configurations we commonly use. As expected, the larger the truncation, the more force required to achieve pressure. The larger the truncation, the more nearly linear the calibration curve.

There is a regular spacing or proportionate gap between the 6 mm and the 8 mm results as pressure increases (Fig. 5). For 6 mm and 8 mm TELs, the size proportion (SP = 8 mm/6 mm) of 1.33 compares to the force proportion (FP = 322/222 tons) of 1.45 for Bi III–V. The regular gap grows for the 8 mm and 12 mm results. The larger SP of 1.50 now requires a proportionately larger FP of 1.59 to achieve Bi III–V. For the 12 mm–19 mm gap comparison, an even larger SP of 1.58, however, only requires a very small FP of 1.24 to achieve Bi III–V. Clearly the finless 19 mm configuration is considerably more efficient at generating pressure than any of the finned configurations. The "finless," make-your-own-gasket-by-extrusion strategy is currently underexplored.

HIGH-TEMPERATURE CALIBRATIONS

Pressure calibration of multianvil presses typically uses multiple quenched experiments to bracket phase transitions at selected pressures at high temperature. More recently, Li and Li[5] used ionic conductivity measurements to detect melting of NaCl *in situ*, with the advantage that multiple pressure points could be calibrated with a single loading and the bracketing could be more precise with repeated crossing of the solid-liquid boundary at each pressure examined. We first explore the results of conventional load-and-quench calibrations for $CaGeO_3$ garnet-perovskite,[6,7] SiO_2 quartz-coesite-stishovite,[8,9] and Mg_2SiO_4 forsterite-wadsleyite-ringwoodite-bridgmanite + periclase[10,11] transitions

(Tables II and III). Then, we examine some of the features of calibration experiments, in which multiple melting and freezing cycles are conducted at several pressures in a single loading (Table IV).

LOAD-AND-QUENCH CALIBRATION OF SOLID-STATE PHASE TRANSITIONS

Figure 6 shows the 1200 °C $CaGeO_3$ calibrations for 6 mm, 8 mm, and 12 mm TELs at 60 kbar, as well as the 1100–1500 °C SiO_2 calibrations for 8 mm and 12 mm TELs at 31–36 kbar, given in Table II. The dashed lines are the room temperature Bi calibrations from Fig. 5. The solid lines for hot calibration are below the dashed lines for the same TEL, showing that it takes more force to reach pressure at high temperature than it does at room temperature. These calibration experiments were undertaken across two laboratories with a variety of heaters ($LaCrO_3$, Re, Ta, and FeCrAlloy) and sample configurations, yet there is a good separation of the fields of the low-pressure polymorph (unfilled symbols) from the high-pressure polymorphs (filled symbols). Evidently the loss of pressurization efficiency is not sensitive to the heater type and details of the configuration. This efficiency gap in hot sample pressurization is also typical of the 584-pressure medium.[2] It appears that the efficiency gap grows with TEL, suggesting that the more pressure medium there is to soften and flow, the greater the loss of efficiency. In Fig. 5 it was clear that there was curvature to the force vs pressure achieved in the room temperature Bi calibrations, meaning there was less efficiency at high pressure as the gaskets became more fully loaded and provided a larger area of support. There was also a systematic decrease in the curvature with larger TEL, seen as progressively smaller values of the quadratic coefficients in Fig. 5 as TEL increased. Here at 1100–1500 °C with the 8 mm and 12 mm TEL, where we have enough coverage and resolution with both SiO_2 and $CaGeO_3$, it is not possible to resolve any departures from a linear relation between force and pressure in this modest pressure range. The 12 mm TEL relation may even be slightly concave up, suggesting a small gain of efficiency at higher pressure. We shall return to this issue below in the section on *in situ* calibration by NaCl melting.
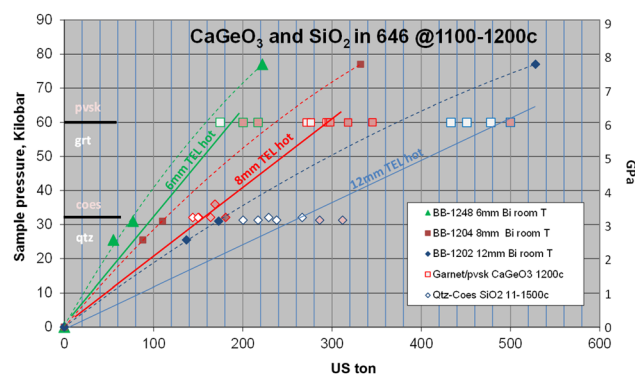

FIG. 6. High-temperature load-and-quench calibrations for $CaGeO_3$ and SiO_2 in 646. Abbreviations: quartz (qtz), coesite (coes), garnet (grt), perovskite (pvsk).

TABLE II. High temperature SiO_2 and $CaGeO_3$ calibrations in cast octahedra with integral fin gaskets.[a]

Serial no.	TEL (mm)	Heater	˚C	US ton	Phase	P (GPa)
			SiO_2 calibrations in 646			
BB-1404	8	Ta	1200	144	qtz	3.2
BB-1405	8	Ta	1200	151	qtz	3.2
M071219	8	Re	1200	150	qtz+coes	3.2
BB-1406	8	Ta	1200	164	qtz+coes	3.2
M071519	8	Re	1500	169	qtz+coes	3.6
BB-1408	8	Ta	1200	181	coes	3.2
BB-1392	12	FeCrAl	1100	200	qtz	3.1
BB-1393	12	FeCrAl	1100	217	qtz	3.1
BB-1394	12	FeCrAl	1200	229	qtz	3.2
BB-1391	12	FeCrAl	1100	238	qtz	3.1
BB-1395	12	FeCrAl	1200	267	qtz	3.2
BB-1390	12	FeCrAl	1100	286	coes	3.1
BB-1389	12	FeCrAl	1100	312	coes	3.1
			$CaGeO_3$ calibrations in 646			
GG-1191	6	LCO	1200	177	garnet	6.0
GG-1193	6	LCO		202	pvsk	6.0
GG-1194	6	LCO		226	pvsk	6.0
BB-1240	8	LCO	1200	269	garnet	6.0
M030716	8	Re/LCO	1200	273	garnet	6.0
BB-1412	8	Ta	1200	294	garnet	6.0
BB-1237	8	LCO	1200	295	pvsk	6.0
M022916	8	Re/LCO	1200	298	pvsk	6.0
BB-1413	8	Ta	1200	318	pvsk	6.0
BB-1238	8	LCO	1200	338	pvsk	6.0
BB-1271	12	LCO	1200	433	garnet	6.0
BB-1272	12	LCO		451	garnet	6.0
TT-1113	12	LCO		478	garnet	6.0
TT-1112	12	LCO		500	pvsk	6.0
			SiO_2 calibrations in 584			
GG-72	8	Re	1200	376	coes+stish	9.3
M102413	8	Re	1200	347	coes+stish	9.3
M070113	8	Re	1200	108	qtz	3.2
			$CaGeO_3$ calibrations in 584			
M073014	8	Re	1200	213	garn+pvsk	6.0

[a]qtz = quartz, coes = coesite, stish = stishovite, garn = garnet, pvsk = perovskite, LCO = doped lanthanium chromium oxide, FeCrAl = FeCrAlloy

The identification of garnet or perovskite polymorphs of $CaGeO_3$ in the experimental products was initially determined from vague morphological suggestions of cubic or dodecahedral habit in a polished section. The results were confirmed by distinct Raman spectra of the polished grains recovered at room pressure and temperature (Fig. 7). The refractive indices for $CaGeO_3$ polymorphs would easily allow the determination as well, except that immersion oils of sufficiently high index are not routinely available. For quartz and coesite in SiO_2 determinative immersion oils are readily available and can be used to distinguish between SiO_2 polymorphs when Raman and IR spectroscopy are not available.

The ambiguities of crystal morphology and the possible unavailability of IR or Raman spectroscopy provide an incentive for finding additional diagnostic criteria for polymorphs of $CaGeO_3$.

There is a simpler diagnostic test for the recovered polymorph which did not require any sample preparation. The garnets are bright white and the perovskites are pale tan/pink, for charges wrapped in Pt foil, a fact that should aid the determination of pressure calibrations with $CaGeO_3$, as seen in Fig. 8.

Pressure calibrations of 5 mm and 3 mm TEL using pyrophyllite gaskets on COMPRES or 646 octahedra are seen in Fig. 9 and Table III. Mg_2SiO_4 forsterite was the starting material. The wadsleyite-ringwoodite result for 3 mm TEL demonstrates that 646 can generate sample pressures greater than 20 GPa because experiment M080319 (Table III) produced ringwoodite rather than wadsleyite at ~1500 ˚C. However, with 3 mm TEL, 646 media failed to covert ringwoodite into bridgmanite at the press load where bridgmanite was produced using the COMPRES

TABLE III. High temperature Mg_2SiO_4 calibrations in finless octahedra with pyrophyllite gaskets.

Experiment ID	TEL	US ton	GPa	T (C)	Product	Heater
			646			
M080119	5	451	<14.3[11]	1400	fo	Re
			>20.3[11]			
M080319	3	715	<23.3[10]	~1500	rw	Re
			COMPRES			
M071619	5	410	<15.1[11]	1600	fo	Re
M071719	5	450	>15.1[11]	1600	wd	Re
M080819	5	496	17.1[11]	2200	fo/wd	LaCrO$_3$
M101319	5	714	<21.0[11]	1600	wd	Re
			>20.5[11]			
M071115	3	525	<23.3[10]	1523	rw	Re
M022819	3	588	23.1[10]	1600	rw/bm+pc	Re
M072913	3	854	>23.3[10]	1500	bm+pc	Re

TABLE IV. High temperature NaCl melting calibrations in octahedra with integral fin gaskets for 8 mm TEL WC anvils.[a]

584 M100313			646 M022219		
US ton	Melting T (°C)	NaCl (GPa)	US ton	Melting T (°C)	NaCl (GPa)
131	1279	3.0	100(1)	1195(7)	2.3
164	1446	4.8	133(1)	1313(4)	3.3
197	1518	5.8	169(1)	1417(4)	4.5
230	1577	6.7	206(2)	1495(7)	5.5
263	1638	7.6	245(2)	1575(7)	6.6
295	1682	8.4	286(3)	1637(18)	7.6
328	1720	9.1	328(2)	1720(20)	9.1

[a]Numbers in parentheses are uncertainties in the last digits, calculated from one sigma of multiple measurements.

media. Moreover, the forsterite-wadsleyite results for 5 mm TEL show 646 to be less efficient than COMPRES media by about 2 GPa near 15 GPa.

IN SITU CONDUCTIVITY CALIBRATION ALONG A MELTING CURVE

On the basis of an established melting curve of NaCl,[12] the *in situ* conductivity method[5] has been applied to determine the relations between sample pressure and press load for 8 mm TEL experiments using cast 584 and 646 octahedra with fins (Table IV and Fig. 10).

All the experiments were conducted using the 1000-ton Walker-style multianvil press at the University of Michigan and used Re heater and Fansteel tungsten carbide (WC) cubes. As described by Li and Li,[5] NaCl powder from Aldrich (99.99%, no.38,886-0) was dried in a vacuum oven at 110 °C before being packed inside a Pt container. A pair of Pt wires of 0.20 mm diameter were inserted into a four-bore alumina holder and used as electrodes. An excitation voltage of 0.1 VAC (alternating current voltage) was applied to the measurement circuit, and the current through the sample was monitored using a Fluke 289 multimeter. Melting was detected on the basis of a steep increase in ionic conductivity upon heating. At each press load, the sample was heated at a rate of 60 °C per min until melting was detected, and then cooled rapidly to ~800 °C to complete one cycle. The cycle was repeated at least once before compressing to the next press load. At the highest load and temperature, the sample was quenched by turning off the heating power. The experimental product was recovered and inspected using a Zeiss optical microscope and a JOEL scanning electron microscope.

In the 584 experiment (M100313, Table IV), a type-C thermocouple of 0.13 mm diameter was used to monitor the temperature. The electrode and thermocouple wires were inserted axially into the cylindrical heater from the opposite ends. The electrode tips and thermocouple junction were placed at the same distance to the equator of the heater, and kept within the middle third of the heater length, where the temperature variation was expected to be <100 °C. The experimental product was inspected to ensure that the electrode tips and the thermocouple junction were positioned symmetrically as expected, and therefore the temperature measurements were validated. Press loads were selected at 40–100 bars, with 10-bar intervals, corresponding to 131 to 328 US tons (Table IV).
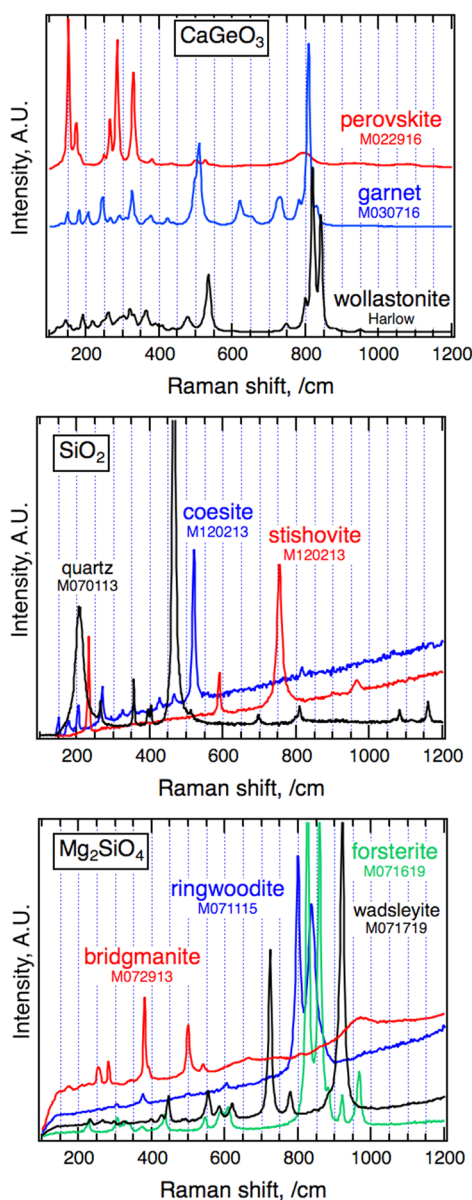
FIG. 7. Raman spectra of starting materials and products of calibration experiments. The spectra were collected using a Renishaw Raman microscope, with 532 nm unpolarized laser light, a 50× objective (2 μm area) in the nonfocal mode, and an 1800 l/mm grating. The collection time ranged between 1 and 60 s. Results are shown without background subtraction.

The 646 experiment (M022219) used a type-S thermocouple of 0.20 mm diameter to monitor the temperature. The electrode and thermocouple wires were inserted into single four-bore alumina tubing, which was then inserted axially into the cylindrical heater from one side. The electrode tips and thermocouple junction were located in a plane parallel to and near the heater equator. This configuration ensured that the temperature and conductivity signals originated from the same region of the sample. Press loads were
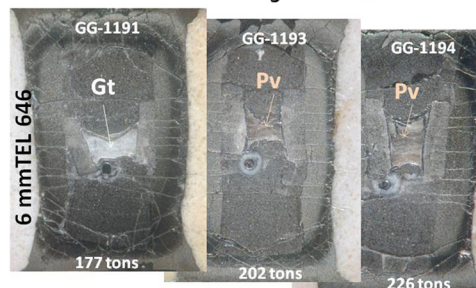

FIG. 8. CaGeO$_3$ polymorphs wrapped in Pt display color differences: garnet is white, perovskite is tan/pink.

selected to produce 3–9 GPa sample pressure with 1 GPa intervals, for 584 pressure media, according to the results of load-and-quench calibration experiments using SiO$_2$ and CaGeO$_3$ transitions (Table III and black line in Fig. 10).

The pressure of NaCl at a given press load is calculated from the measured melting temperature using Simon's equation $(T/T_0)^c = (P - P_0)/A + 1$, where $T_0 = 1073.6$ K and T (in Kelvin) are
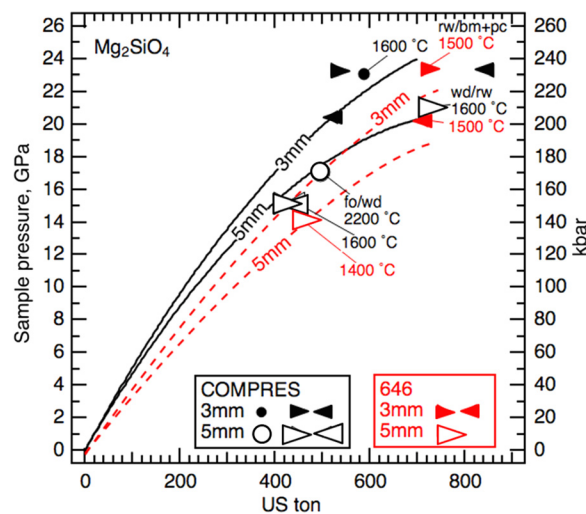

FIG. 9. High temperature calibrations using Mg$_2$SiO$_4$ starting materials for 3 mm and 5 mm TEL octahedra with pyrophyllite gaskets. Data are found in Table III. The results of experiments using COMPRES injection molded octahedra (black symbols) are in good agreement with the black curves reproduced from Leinenweber *et al.*[3] The results of experiments using 646 cast octahedra (red symbols) are used to constrain the red dashed curves. Circles denote two phases coexisting. Left- and right-pointing wedges denote single phases at higher tonnage or lower tonnage, respectively, than the relevant phase boundary at the experimental temperature. In experiment M080319, ringwoodite was the product at 715 tons and 1500 ˚C. The two red-filled wedges indicate that the tonnage was above that required for the rw/wd transition at 20.3 GPa and below that required for the rw/bm + pc transition at 23.3 GPa. Thus, sample pressure is greater than the 20.3 GPa needed for the rw/wd boundary and less than the 23.3 GPa needed to achieve the rw/bm + pc boundary. Abbreviations: forsterite (fo), wadsleyite (wd), ringwoodite (rw), bridgmanite (bm), periclase (pc).
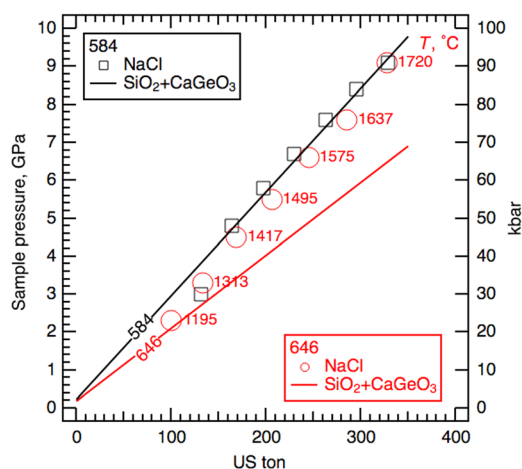
FIG. 10. Pressure calibrations of 8 mm TEL anvils based on the melting curve of NaCl. Black (584) and red (646) lines are linear fits to load-and-quench calibration experiments using SiO_2 and $CaGeO_3$ (Table III). Red circles and black squares represent pressures determined from the melting temperatures of NaCl (marked next to the 646 data points) at various press loads.

the melting temperatures at the reference pressure $P_0 = 1$ bar $= 0.0001$ GPa and P (in gigapascal), respectively. Fitting the reported data of Akella et al.[12] up to 6.5 GPa yielded $c = 1.06$ and $A = 3.65$ (Li and Li[5]).

For 584, the NaCl pressures match well with the load-and-quench, single cycle calibration line, except at 140 ton, where the NaCl pressure is lower by more than 1 GPa (Fig. 10). For 646, the NaCl pressure is always below the load-and-quench 584 calibration line (black line) except at the highest load where both generated ~9 GPa (Fig. 10). This is consistent with the cold calibrations of Figs. 2 and 3 where 646 is consistently less efficient at pressurization than 584. The first heating cycle of 646–1195 °C in Fig. 10 gives a result very close to the red 1200 °C load-and-quench single cycle calibration curve of Fig. 6, as expected, and indeed as required, if results are to be claimed to be reproducible. However subsequent heating cycles at increasing pressure, reaching successively higher temperatures, show convergence with the 584 load-and-quench and in situ NaCl melting result for 584 (black line). Evidently there is some complexity of behavior which is influenced by pressure, temperature, and process cycling.

A previous study using in situ synchrotron x-ray diffraction showed that, at a fixed press load, sample pressure decreased by 1–2 GPa when the sample was heated from 1200 °C to 1600 °C (Fei et al.[10]) However, the same study showed that at a given press load, sample pressure increased by about 2 GPa between 1200 and 2000 °C after a temperature cycle. More complex behaviors of pressure variation with temperature at fixed press loads were observed in another synchrotron x-ray diffraction study, where sample pressure decreased by more than 5 GPa between room temperature and 1200 °C in an experiment using the COMPRES 8/3 on-line assembly and varied by about ±1 GPa between room temperature and 1500 °C in an experiment using the COMPRES 10/5 on-line assembly (Leinenweber
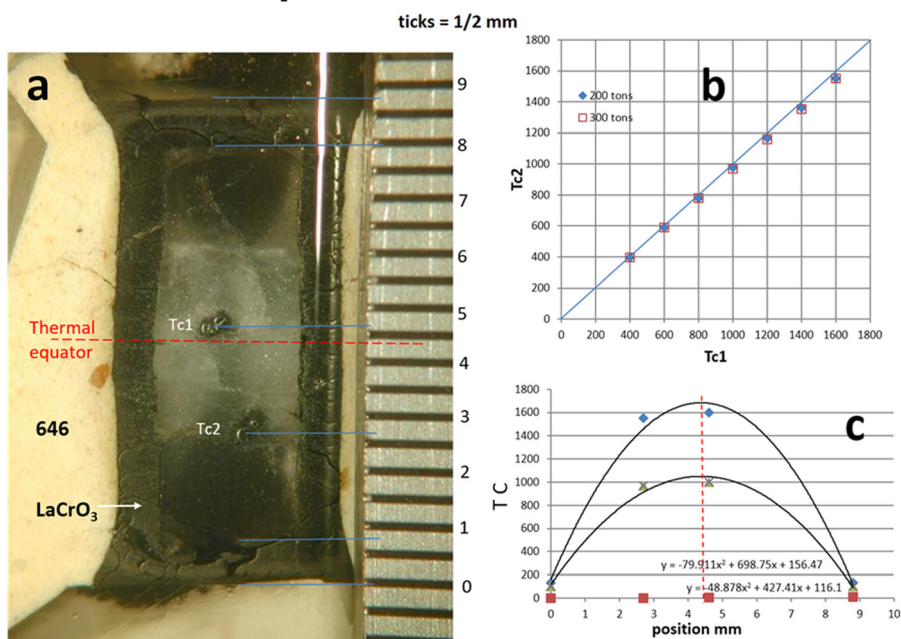

FIG. 11. Thermal structure in 8 mm 646 assembly with LaCrO₃ heater determined by two independent thermocouples 2 mm apart.

et al.[3]) Our results of Bi calibration and high-temperature calibrations support the general observation that sample pressure tends to decrease with increasing temperature, and this behavior can be understood by the softening and extrusion of the pressure medium at high temperatures. While temperature cycling seems a plausible explanation for the divergence of NaCl pressure from the load-and-quench calibration curve in the 646 experiment, the same is not observed in the 584 NaCl experiment. We do not know why 646 improves its pressurization efficiency at higher temperatures and possibly with cycling whereas 584 does not. Perhaps the better thermal insulation provided by 646 helps to keep the gaskets of the pressure medium cool and so reduce thermal relaxation and maintain thermal pressure, whereas a larger volume of the 584 assembly is heated to temperatures that allow gasket creep regardless of the temperature and cycling history.

While the *in situ* conductivity calibration method using NaCl has the distinct advantage of high efficiency and more precise bracketing, its resolution diminishes at high pressures where the melting slope becomes small, and therefore, the melting temperature becomes less sensitive to pressure. With NaCl, the melting slope changes from 200 °C/GPa at low pressures to 20 °C at 15 GPa, and therefore it would no longer be a good candidate for pressure calibration above 10 GPa.

THERMAL STRUCTURE

The superior thermal insulating properties of 646 castable ceramic reflect its zirconia base. The thermal conductivity of ZrO_2 (1.8–2.2 W/m-K) is ten times smaller than that of Al_2O_3 (40 W/m-K) or MgO (28–35 W/m-K) at 1 bar and 300 K (Clauser and Huenges[13]). Only about ~60% of the power consumption required to achieve 1200 °C with Re heaters and $LaCrO_3$ liners in 8 mm TEL 584 pressure media (265 W) is needed to produce the same temperature with 646 pressure media (158 W). The thermal structure of experiments in 646 with $LaCrO_3$ heaters is similarly efficient and is more favorable for achieving low-gradient T distributions than Re. Figure 11(a) shows the sectioned product of experiment BB-1244 with a $LaCrO_3$ heater and two thermocouples, one at the thermal equator and one 2 mm off the hot spot. The temperature difference between these widely separated thermocouples is only 50 °C or less at 1600 °C, as shown in Fig. 11(b). The gradient is substantially flatter than the quadratic fitting function near the hot zone of the furnace, as shown in Fig. 11(c). Clearly, part of this low T gradient character is attributable to the semiconductor behavior of the $LaCrO_3$ that dissipates more power in the high resistance, cool regions, away from the hot spot of the thermal equator. The superior insulation of the 646 keeps the extra dissipated heat from leaking out more effectively than a poor insulator would, thereby promoting the more uniform T distribution, as well as heating efficiency.

SUMMARY

Castable ceramics, compared to machined or injection molded pressure media, can be fabricated into intricate shapes without undue repetitive effort once a mold has been formed. Their ability to be cast with integral gasket fins avoids the steps of cutting and placement of pyrophyllite gaskets. This simplifies the assembly of experiments and reduces the complexity of the supply chain. Different castable

compounds have different strengths and weaknesses. Our exploration over the years of Ceramacast 584 and 646 reveals that, in general, 584 is superior in efficiently translating press force into sample pressurization; in some cases, it is slightly more efficient than the standard machined or injection molded multianvil pressure media with pyrophyllite gaskets. The appeal of the less pressure-efficient 646 includes its ease of casting and fabrication. Its superior thermal insulation conserves power and protects the anvils and lubricating plastic pads from thermal damage at high experiment temperatures better than the alternatives. However, the performance of castable 584 and 646 ceramics with integral fin gaskets above 10 GPa is not as reliable as the standard ceramic+pyrophyllite gasket assemblies in preventing blowouts. This suggests the use of castable ceramic octahedra with pyrophyllite gaskets as a substitute for the more costly machined or injection molded standard materials at pressures above 10 GPa. Our study shows that even the pressure-inefficient 646, when used with pyrophyllite gaskets, can be competitive with other standard materials in pressure generation at lower cost and with better thermal insulation.

APPENDIX: REFERENCE PRESSURE OF THE BI II-III TRANSITION

Where should the Bi II–III transition be found? Here we explain why we use 31 kbar instead of the equilibrium value of 27 kbar[14] for this transition at room temperature. Decker *et al.*[4] are silent on where Bi II–III occurs, dismissing it as irrelevant to adding new information to calibration exercises because it is so close to the Bi I–II transition at 25.5 kbar. They mention it only in passing in their section on transitions between 30 and 80 kbar. Efforts to refine the equilibrium Bi II–III transition have mostly been concerned with reducing the hysteresis of compression-decompression cycles.[15–17] These efforts underline that Bi I–II and II–III are indeed close together and do show appreciable hysteresis between compression and decompression cycles which is reduced by slow cycling. Multianvil experiments typically achieve pressurization in hours compared to equilibrium-seeking experiments lasting days; and multianvil presses typically operate with advancing-anvil-only compression rather than pressure-cyclic paths. Thus, transitions will be smeared and offset to higher than expected pressures. For these reasons, the equilibrium values for the transition may not be relevant to the signals monitored in multianvil situations. Figure 12 shows a compression trace of a 4 mm long cylinder of Bi of 1.5 mm outside diameter (OD) monitored by a four-wire resistance measuring circuit. The features include two areas
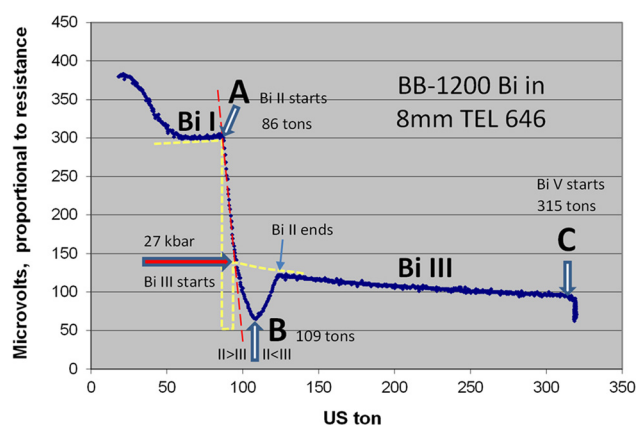
FIG. 12. Resistance of Bi as a function of press load for an 8 mm TEL octahedron with integral gaskets cast from 646 ceramic. Abrupt resistance changes correspond to phase changes between Bi polymorphs. Red dashed line is the initial linear slope of the Bi I–II transition. Yellow dashed trace, based on Bundy,[14] is the theoretical trace if the transformations were instantaneous and without hysteresis. The real trace, BB-1200, taken over 17 h exhibits smearing of the Bi II stability to higher-than-equilibrium pressures.

of slowly changing resistance, corresponding to stable areas labeled Bi I and Bi III. Between these plateaux, from 86 to 125 tons, is an asymmetric V-shaped valley of roughly the depth and position (but not the shape) expected for the stability of Bi II. The left flank of the valley is initiated by the precipitous drop in resistance as Bi I transforms to Bi II. It is clear from the fact that there is a slope to the valley side that the transformation is not instantaneously complete. There is some smearing of the transition across a range of pressures, in contrast to the expectation that the transition in pure Bi at one temperature should be isobaric, as illustrated by the yellow trace. If there were no smearing, then the valley side would be vertical, the floor corresponding to Bi II would be flat, and the right flank would rise vertically to recover the higher resistance for Bi III when it emerges. Such plots may be found in Bundy[14] who did not conduct the rapid compressions of multianvil experiments.

A, B, and C correspond to the features commonly picked by the white arrows as Bi I–II, Bi II–III, and Bi III–V on such Bi resistance traces. If standard pressures of 25.5, 31, and 77 kbar are assigned to these transitions, one gets the calibration curves of Figs. 2–6. Using the calibration formula shown in Fig. 2 for BB-1200, one may compute the tonnage at which the pressure ought to be 27 kbar, shown here with the red arrow. This 27 kbar point corresponds to a divergence in slope of the Bi I–II transition from its initial linearity (red dashed line) at the left head of the valley. Because 27 kbar is the pressure expected for the transformation of Bi II-III to begin, it is reasonable to interpret this divergence as the arrival of Bi III, which introduces a diminution of the rate of decrease of the resistance caused by the growth of Bi II at the expense of high-resistance Bi I. The less-steep, lower-left flank of the V-shaped valley reflects the substitution of Bi III for Bi I, although the exact point at which Bi I disappears cannot be determined. What is clear is that when the minimum resistance of the bottom of the V-shaped valley is passed, the upward climb of the trace reflects the shrinking contribution of low-resistance Bi II, as Bi III becomes the major phase. At the right

head of the valley, entering the Bi III plateau, Bi II is exhausted. It is clear from this analysis that the arrival of Bi III is difficult to pin point, although the break in slope at the red arrow at 27 kbar is a plausible marker when resolvable. However, the bottom of the V is easily recognized and resolved, and very reproducibly located at 31 ± 1 kbar in multianvil speed compressions. This is the reason for adopting 31 kbar for Bi II–III in multianvil compressions. More properly, it is the point at which the growth of Bi III outpaces the consumption of Bi II, rather than the equilibrium transition pressure, which can still be recognized at 27 kbar on favorably stable traces. These same resistance trace features are widely recognized in the multianvil community. The Bi II–III is just as widely ignored. For instance, Knibbe et al.[18] picked the bottom of the V as the Bi II–III transition, but they did not plot it as a calibration point at 27 kbar because it would have fallen off their curve from Bi I–II and Bi III–V. Use of 31 kbar would have fit nicely. The analysis of Fig. 12 provides justification for such a choice. Figure 13 provides a visual confirmation of how poorly the choice of 27 kbar works for the bottom of the V being a proxy for the equilibrium Bi II–III transformation.

Smearing of the univariant Bi transitions over a pressure interval of several kilobars is indicated by the slopes of the transitions in Fig. 12, and by the absence of any clear, flat, Bi II-only floor in the V-shaped valley of Bi II. The yellow trace shows the expected resistance for a full instantaneous transformation upon compression without smearing, to higher pressure. What causes this smearing? One factor could be sluggish transformation kinetics, and indeed, refinement studies[15–17] indicate that some overshoot in pressure is needed to initiate the transitions, especially in fluid media. Overshoot delay is distinguishable from a kinetically sluggish transformation progress, once initiated. We believe that the reproducibility of replicate calibrations done across two different labs with somewhat different loading protocols suggests that Bi transformation sluggishness and delayed nucleation are not the most important factors. Delayed nucleation is also hard to reconcile with the break in slope seen at the expected pressure for Bi III onset of 27 kbar based on Bi I–II and Bi III–V in Fig. 12. Intrinsic to any solid medium pressure device is the possibility of nonuniform pressure within the cell, especially at low temperature, where pressure media are stronger and
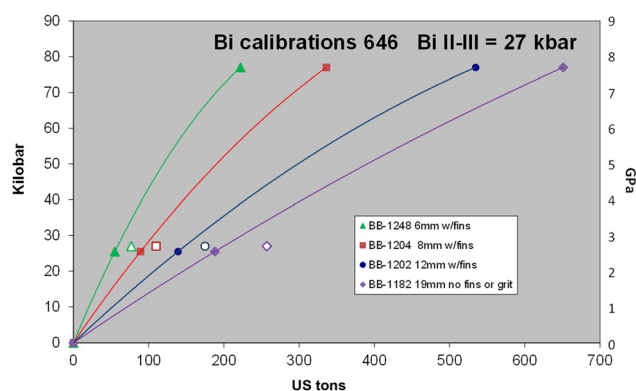

FIG. 13. Shows the Bi calibrations of Fig. 5, except that Bi II–III, plotted as open symbols for the tonnage at the lowest point of the V valley, is plotted at 27 kbar instead of 31 kbar. It is clear that the open symbols fall systematically off and below the calibration curves shown here, which are based on fitting the standard values of Bi I–II = 25.5 kbar and Bi III–V = 77 kbar.

able to maintain stress and pressure gradients as loading proceeds. Thus, the pressurization process may produce Bi charges in which the whole charge is not at uniform pressure. As pressurization proceeds, isobars may sweep through the charge, which could lead to equilibrium phase pairs in the Bi, in addition to the presence of metastable phases due to kinetic effects. The smearing of the transitions during pressurization could arise from pressure gradients within the assembly. As the ceramic media are much stronger than the Bi, the time scale for relaxation towards pressure uniformity, and vertical valley trace sides, is set by the pressure medium, not the Bi. An additional feature of Fig. 12 worth noting is the abrupt and vertical resistance change seen at greater than 315 tons, where the characteristic break in slope for the Bi III–V transition is observed. Pressurization to 319 tons took 12 h. The pressure was then maintained at 319 tons without any further increase of pressure for an additional 5 h, during which the transformation to Bi V was completed. Thus, at very, very slow pressurizations the pressure medium can relax its wrinkles to promote full conversions without excessive pressure smearing of the transition. This of course would be a counterproductive procedure to adopt when the objective is experimental throughput. We calibrated for the typical loading rates and holding times of our experiments. These considerations diminish at high temperature where hold and quench transitions usually yield complete conversions rapidly.

REFERENCES

[1] R. C. Liebermann, "Multi-anvil high pressure apparatus: A half-century of development and progress," High Pressure Res. **31**, 493 (2011).

[2] D. Walker, "Lubrication, gasketing and precision in multianvil experiments," Am. Miner. **76**, 1092 (1991).

[3] K. D. Leinenweber, J. C. Tyburczy, T. C. Sharp, E. Soignard, T. Diedrich, W. B. Putuskey, Y. Wang, and J. L. Mosenfelder, "Cell assemblies for reproducible multi-anvil experiments (the COMPRES assemblies)," Am. Mineral. **97**, 353 (2012).

[4] D. L. Decker, W. A. Bassett, L. Merrill, H. T. Hall, and J. D. Barnett, "High-pressure calibration: A critical review," J. Phys. Chem. Ref. Data **1**, 773 (1972).

[5] Z. Li and J. Li, "Melting curve of NaCl to 20 GPa from electrical measurements of capacitive current," Am. Mineral. **100**, 1892 (2015).

[6] J. Susaki, M. Akaogi, S. Akimoto, and O. Shimomura, "Garnet-perovskite transformation in $CaGeO_3$: *In situ* X-ray measurements using synchrotron radiation," Geophys. Res. Lett. **12**, 729, https://doi.org/10.1029/JZ067i002p00851 (1985).

[7] S. Ono, T. Kikegawa, and Y. Higo, "*In situ* observation of a garnet perovskite transition in $CaGeO_3$," Phys. Chem. Miner. **38**, 735 (2011).

[8] K. Bose and J. Ganguly, "Quartz-Coesite transition revisited: Reversed experimental determination at 500–1200 °C and retrieved thermochemical properties," Am. Miner. **80**, 231 (1995).

[9] J. Zhang, B. Li, W. Utsumi, and R. C. Liebermann, "*In situ* X-ray observation of the Coesite-Stishovite transition: Reversed phase boundary and kinetics," Phys. Chem. Miner. **23**, 1 (1996).

[10] Y. Fei, J. A. Van Orman, J. Li, W. van Westrenen, C. Sanloup, W. Minarik, K. Hirose, T. Komabayashi, M. Walter, and K. Funakoshi, "Experimentally determined postspinel transformation boundary in Mg_2SiO_4 as an internal pressure standard and its geophysical implications," J. Geophys. Res. **109**, B02305, https://doi.org/10.1029/2003JB002562 (2004).

[11] T. Katsura and E. Ito, "The system Mg_2SiO_4–Fe_2SiO_4 at high pressures and temperatures: Precise determination of stabilities of olivine, modified spinel, and spinel," J. Geophys. Res. **94**, 15663, https://doi.org/10.1029/jb094ib11p15663 (1989).

[12] J. Akella, S. N. Vaidya, and G. C. Kennedy, "Melting of sodium chloride at pressures to 65 kbar," Phys. Rev. **185**, 1135 (1969).

[13] C. Clauser and E. Huenges, "Thermal conductivity of rocks and minerals," in *Rock Physics and Phase Relations: A Handbook of Physical Constants*, edited by T. Ahrens, (AGU Reference Shelf, 1995), Vol. 3.

[14] F. P. Bundy, "Phase diagram of Bismuth to 130 000 kg/cm^2, 500 °C," Phys. Rev. **110**, 314 (1958).

[15] G. C. Kennedy and P. N. LaMori, "The pressures of some solid-solid transitions," J. Geophys. Res. **67**, 851, https://doi.org/10.1029/JZ067i002p00851 (1962).

[16] M. Nomura, T. Nishizaka, Y. Hirata, N. Nakagiri, and H. Fujiwara, "Measurement of the resistance of Manganin under liquid pressure to 100 kbar and its applications to the measurement of the transition pressures of Bi and Sn," Jpn. J. Appl. Phys. **21**, 936 (1982).

[17] I. C. Getting, "New determination of the bismuth I-II equilibrium pressure: A proposed modification to the practical pressure scale," Metrologia **35**, 119 (1998).

[18] J. S. Knibbe, S. M. Luginbuhl, R. Stoevelaar, W. van der Plas, D. M. van Harlingen, N. Rai, E. S. Steenstra, R. van de Geer, and W. van Westrenen, "Calibration of a multi-anvil high-pressure apparatus to simulate planetary interior conditions," EPJ Tech. Instrum. **5**, 5 (2018).